

Electrochemical behavior and underpotential deposition of Sm on reactive electrodes (Al, Ni, Cu and Zn) in a LiCl–KCl melt

Tai-qi Yin, Lang Chen, Yun Xue, Yang-hai Zheng, Xue-peng Wang, Yong-de Yan, Mi-lin Zhang, Gui-ling Wang, Fan Gao, and Min Qiu

Cite this article as:

Tai-qi Yin, Lang Chen, Yun Xue, Yang-hai Zheng, Xue-peng Wang, Yong-de Yan, Mi-lin Zhang, Gui-ling Wang, Fan Gao, and Min Qiu, Electrochemical behavior and underpotential deposition of Sm on reactive electrodes (Al, Ni, Cu and Zn) in a LiCl–KCl melt, *Int. J. Miner. Metall. Mater.*, 27(2020), No. 12, pp. 1657-1665. <https://doi.org/10.1007/s12613-020-2112-2>

View the article online at [SpringerLink](#) or [IJMMM Webpage](#).

Articles you may be interested in

Gao-jie Li, Ming-xing Guo, Yu Wang, Cai-hui Zheng, Ji-shan Zhang, and Lin-zhong Zhuang, [Effect of Ni addition on microstructure and mechanical properties of Al-Mg-Si-Cu-Zn alloys with a high Mg/Si ratio](#), *Int. J. Miner. Metall. Mater.*, 26(2019), No. 6, pp. 740-751. <https://doi.org/10.1007/s12613-019-1778-9>

Yuan Li, Li-na Cheng, Wen-kang Miao, Chun-xiao Wang, De-zhi Kuang, and Shu-min Han, [Nd–Mg–Ni alloy electrodes modified by reduced graphene oxide with improved electrochemical kinetics](#), *Int. J. Miner. Metall. Mater.*, 27(2020), No. 3, pp. 391-400. <https://doi.org/10.1007/s12613-019-1880-z>

Sreejith J and S. Ilangoan, [Optimization of wear parameters of binary Al-25Zn and Al-3Cu alloys using design of experiments](#), *Int. J. Miner. Metall. Mater.*, 25(2018), No. 12, pp. 1465-1472. <https://doi.org/10.1007/s12613-018-1701-9>

Zhi-hao Zhang, Jie Xue, Yan-bin Jiang, and Feng Jin, [Effect of pre-annealing treatment on the microstructure and mechanical properties of extruded Al-Zn-Mg-Cu alloy bars](#), *Int. J. Miner. Metall. Mater.*, 24(2017), No. 11, pp. 1284-1292. <https://doi.org/10.1007/s12613-017-1521-3>

Mohammad Baghani, Mahmood Aliofkhazraei, and Mehdi Askari, [Cu-Zn-Al₂O₃ nanocomposites: study of microstructure, corrosion, and wear properties](#), *Int. J. Miner. Metall. Mater.*, 24(2017), No. 4, pp. 462-472. <https://doi.org/10.1007/s12613-017-1427-0>

Qing-ling Li, Hua-rui Zhang, Ming Gao, Jin-peng Li, Tong-xiao Tao, and Hu Zhang, [Mechanisms of reactive element Y on the purification of K4169 superalloy during vacuum induction melting](#), *Int. J. Miner. Metall. Mater.*, 25(2018), No. 6, pp. 696-703. <https://doi.org/10.1007/s12613-018-1617-4>



IJMMM WeChat



QQ author group

Electrochemical behavior and underpotential deposition of Sm on reactive electrodes (Al, Ni, Cu and Zn) in a LiCl–KCl melt

Tai-qi Yin^{1,*}, Lang Chen^{1,3,*}, Yun Xue¹, Yang-hai Zheng¹, Xue-peng Wang¹, Yong-de Yan^{1,2}, Mi-lin Zhang¹, Gui-ling Wang¹, Fan Gao², and Min Qiu²

1) College of Materials Science and Chemical Engineering, Harbin Engineering University, Harbin 150001, China

2) College of Science, Heihe university, Heihe 164300, China

3) Geely Automobile Research Institute, Ningbo 315336, China

(Received: 26 April 2020; revised: 30 May 2020; accepted: 1 June 2020)

Abstract: Sm extraction from a LiCl–KCl melt was carried out by forming alloys on various electrodes, including Al, Ni, Cu, and liquid Zn, and the electrochemical behaviors of the resultant metal products were investigated using different electrochemical techniques. While Sm metal deposition via the conventional two-step reaction process was not noted on the inert electrode, underpotential deposition was observed on the reactive electrodes because of the latter's depolarization effect. The depolarization effects of the reactive electrodes on Sm showed the order $Zn > Al > Ni > Cu$. Sm–M (M = Al, Ni, Cu, Zn) alloys were deposited by galvanostatic and potentiostatic electrolysis. The products were fully characterized by X-ray diffractometry (XRD) and scanning electron microscopy (SEM)–energy dispersive spectrometry (EDS), and the stability of the obtained M-rich compounds was determined. Finally, the relationship between the electrode potential and type of Sm–M intermetallic compounds formed was assessed on the basis of the observed electrochemical properties and electrodeposits.

Keywords: electrodeposits; depolarization effect; reactive electrodes; samarium alloys

1. Introduction

Reprocessing of spent nuclear fuel (SNF) is considered a key problem related to the sustainability of nuclear power generation [1]. During pyroprocessing, large amounts of U or U–Pu products are electrodeposited on cathodes for recovery, and fission products left in molten salts are extracted for salt decontamination [2]. When the molten salt reactor is operated, the major fission products, which often include rare earth elements, can form stable fluoride compounds that may corrode the structural materials and affect the properties of the primary salt obtained. Thus, these fission products must be eliminated from the melt to optimize reactor operations [3].

Sm is a fission product of SNF and has been widely studied on various inert and reactive electrodes [2]. Sm may transition from the trivalent state to the divalent state in a molten salt to induce cyclic electrolysis, which could affect the current efficiency of the system [4]. Sm extraction on inert electrodes in chloride [5–6] and fluoride [7–8] melts was first investigated via electrochemical studies and thermody-

amic analysis, and a two-step mechanism was discovered. In this mechanism, the second step occurs outside of the electrochemical window. Therefore, Sm extraction can be only realized on reactive electrodes in molten salts. The shifting of the potential of Sm toward positive values is attributed to the lowering of the activity of the element in the reactive metal phase to form stable Sm-based alloys [9]. Al presents excellent properties and has been widely applied to different fields, such as the aviation industry [10–13] and batteries [14–17]. Some studies on Sm extraction have focused on this metal's combination with Al. Electrochemical studies on Sm have also been conducted in LiF–CaF₂–AlF₃–Sm₂O₃/SmF₃ melts on an inert electrode [7,18], as well as in LiCl–KCl–SmCl₃/Sm₂O₃–AlCl₃ on an Al electrode [19–21]; in these studies, the main products were usually Al₃Sm or Al₂Sm. Ni, as a remarkable reactive metal, could be employed in LiF–CaF₂ melts [8,22]; in this case, a mixture of Ni₂Sm and Ni₃Sm may be obtained under different current densities. NiSm, Ni₂Sm, and Ni₃Sm could be prepared from LiCl–KCl melts by using different potentials [23]. Taxil *et al.* [24] in-

*These authors contributed equally to this work.

Corresponding authors: Yun Xue E-mail: xueyun@hrbeu.edu.cn; Yong-de Yan E-mail: y5d2006@hrbeu.edu.cn

© University of Science and Technology Beijing and Springer-Verlag GmbH Germany, part of Springer Nature 2020

produced Cu as a reactive electrode to extract Sm from the LiF–CaF₂ system; here, a mixture of Cu₄Sm, Cu₅Sm, and Cu₆Sm was formed by galvanostatic electrolysis at 1113 K. Besides solid reactive electrodes, liquid Zn electrodes may also be employed in LiCl–KCl–SmCl₃ systems. For example, previous investigations clearly showed the formation of Zn₁₂Sm and Zn₁₇Sm₂ on Zn electrodes by potentiostatic electrolysis at 873 K [25].

Sm may be combined with other metals to improve the properties of the primary material. Indeed, a number of physical properties, including micro-hardness and corrosion resistance, could be remarkably improved by the metal's ability to form whiskers [26]. Rare-earth elements may be combined with a reactive metal as a transition alloy to form a new material. Iida *et al.* [27], for instance, studied Ni–Sm alloy films. While only Ni₂Sm could be obtained under various applied potentials, Ni₃Sm and Ni₅Sm could be formed on Ni₂Sm electrodes by anodic potentiostatic electrolysis. Magnetic Ni–Sm alloys could be prepared from LiCl–KCl–SmCl₃–NiCl₂ melts on inert electrodes [28]; here, different intermetallic compounds, including NiSm, Ni₂Sm, and Ni₅Sm, may be obtained by coreduction. Electrochemical synthesis of Cu–Sm dendritic alloys for use as catalysts may be carried out by coreduction in LiCl–KCl–SmCl₃–CuCl₂ melts [29] to produce CuSm, Cu₅Sm, and Cu₆Sm under various applied potentials.

Herein, we examined the electrochemical behavior and underpotential deposition of Sm on various reactive electrodes in a molten salt. The extraction efficiency of Sm strongly depends on the deposition potential [30], depolarization value [31], and stability of the cathodic products [32–33]. In this work, we studied the deposition potential of Sm on reactive electrodes and prepared Sm–M (M = Al, Ni, Cu, Zn) alloys by potentiostatic and galvanostatic electrolysis. The electrochemical behavior of the metal products formed was then determined to provide a feasible method to extract Sm from contaminated salts.

2. Experimental

The electrochemical cell used in this work was designed as a three-electrode system with molten salt, as shown in Fig. 1. The molten salt was composed of LiCl–KCl eutectic salt (>99.0% anhydrous, Xilong Scientific Co., Ltd.) and SmCl₃ (>99.9% anhydrous, Alfa-Aesar). Prior to the experiments, LiCl–KCl blank salt was mixed in an alumina crucible and then heated in a vacuum drying oven at 473 K for over 24 h. Thereafter, the crucible was transferred to a furnace for heating up to the experimental temperature of 773 K. Cyclic voltammetry (CV) was conducted on the blank molten salt to detect impurities in the system. If any impurity was found, pre-electrolysis by potentiostatic electrolysis was conducted at –2.1 V vs. Ag/AgCl until these impurities could no

longer be detected. Next, SmCl₃ was added to the melt, and the actual concentration of Sm was measured using inductively coupled plasma optical emission spectrometry (HORIBA).

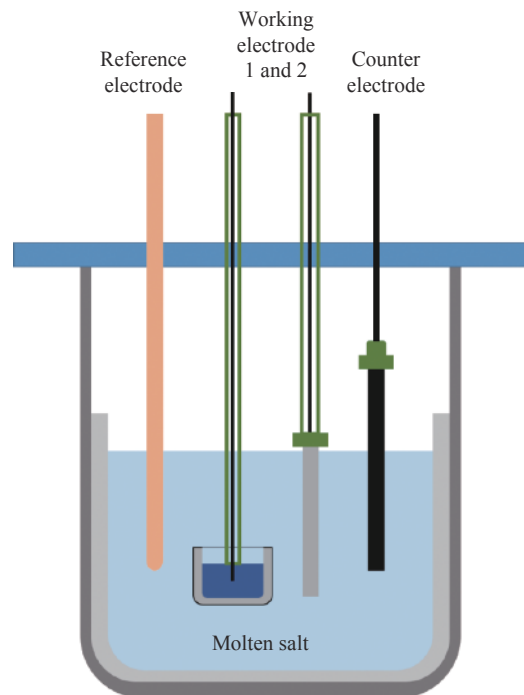


Fig. 1. Illustration of the electrochemical cell.

The working electrode (WE) was made up of various electrodes, including W wire (99.99%, ϕ 1 mm), Al wire (99.99%, ϕ 1 mm), Ni wire (99.99%, ϕ 1 mm), and Cu wire (99.99%, ϕ 1 mm), and liquid Zn granules (99.99%; Sino-pharm Chemical Reagent Co., Ltd.). The reactive Zn electrode, which presented a liquid state at the experimental temperature, was placed in an alumina crucible (ϕ 16 mm \times 16 mm). Mo wire was used as the conductor for the Zn metal and electrode clamp. The reference electrode was made of Ag wire (99.99%, ϕ 1 mm), 1wt% AgCl (99.99%, Alfa-Aesar), and an alundum tube (ϕ 6 mm) containing LiCl–KCl eutectic molten salt. The counter electrode was a graphite rod (ϕ 4 mm) of spectral purity. All experimental tests, including CV, square wave voltammetry (SWV), and open-circuit chronopotentiometry (OCP), were carried out on an Autolab PGSTAT302N potentiostat/galvanostat.

The samples were prepared by galvanostatic or potentiostatic electrolysis. After sonicleaning with distilled water, the alloy samples were placed in a cylinder by using a metallographic sample mounting press, smoothed with sand paper, and then polished with a polisher for further analysis. X-ray diffractometry (XRD; Bruker, D8 Advance) was performed to identify the phase composition of the samples. Scanning electron microscopy (SEM)–energy dispersive spectrometry (EDS; JSM-6480A; JEOL Co., Ltd.) was also carried out to

examine the morphology and elementary composition of the samples.

3. Results and discussion

3.1. Cyclic voltammetry

A typical CV curve obtained on the W electrode after addition of SmCl_3 to the LiCl–KCl eutectic melt is shown in Fig. 2. The A0/A0' peak couple is known to indicate the reduction/oxidation of Li(I)/Li. The B/B' redox signal is characteristic of a soluble–soluble system, which corresponds to the reaction of Sm(III)/Sm(II) [34]. The soluble/insoluble reaction corresponding to the Sm(II)/Sm(0) peak couple could not be determined because the reaction potential is beyond the electrochemical window of the primary salt [6]. The standard reduction potentials of LiCl/Li, KCl/K, and SmCl_2/Sm were determined according to previous thermochemical data [35] and are shown in Table 1. However, the reduction potential of SmCl_2/Sm under the condition of supercooling could not be calculated because of a lack of data. The standard potential of $\text{SmCl}_3/\text{SmCl}_2$ has been reported in the literature [6].

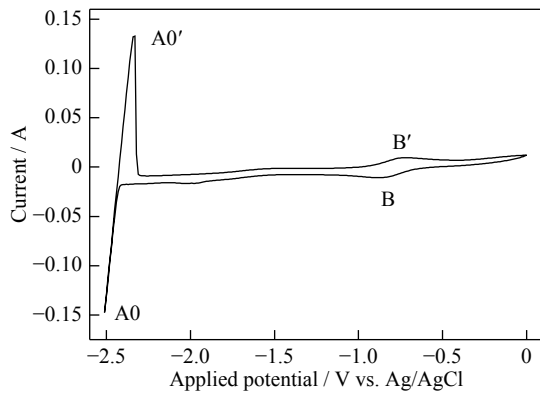


Fig. 2. CV plot obtained after addition of 1wt% SmCl_3 to the LiCl–KCl melt at 773 K. Working electrode: W; scan rate: 0.1 V/s.

Table 1. Standard reduction potentials (E^\ominus) of LiCl/Li, KCl/K, SmCl_2/Sm , and $\text{SmCl}_3/\text{SmCl}_2$

Redox couple	E^\ominus / V vs. Cl_2/Cl^-
LiCl/Li	-3.55
KCl/K	-3.69
SmCl_2/Sm	-3.59
$\text{SmCl}_3/\text{SmCl}_2$	-2.00 ^a

Note: ^a—The value is obtained from Cordoba and Caravaca [6].

Fig. 3 shows four groups of typical CV curves obtained on the reactive solid (Al, Ni, and Cu) and liquid Zn electrodes in the LiCl–KCl–1wt% SmCl_3 melt at 773 K. The Ai/Ai' ($i = 1, 2, 3, 4$) peak couple in Fig. 3 represents the reaction of Li(I)/Li on the different reactive electrodes. The positive shift of potentials shown in Figs. 3(a) and 3(d) is attributed to the underpotential deposition of Al–Li [26] and Zn–Li [25] al-

loys. The most positive peak couples, namely, C/C', D/D', E/E', and F/F', in the different CV curves correspond to the redox signals of Al, Ni, Cu, and Zn, respectively. Besides the redox signals Ai/Ai' and B/B' (Sm(III)/Sm(II)) and the peak couples of the reactive metals, several other pairs of signals could be attributed to the formation of Sm–M intermetallic compounds. The phase diagram of the Al–Sm system, for example, reveals that five intermetallic compounds could be obtained [36]. However, only one redox signal, G/G', is observed in Fig. 3(a). Moreover, two pairs of signals, namely, H/H' and I/I', which correspond to the formation of Ni–Sm intermetallic compounds, are shown in Fig. 3(b), but eight intermetallic compounds should exist according to the Ni–Sm phase diagram [37]. Thermodynamic evaluation of the Cu–Sm system [38] reveals that five intermetallic compounds should be formed. However, only two pairs of signals, J/J' and K/K', were correlated with Cu–Sm intermetallic compounds. These results may be attributed to the slow growth of other phases [39]. The redox signal of Sm(III)/Sm(II) on the liquid Zn electrode cannot usually be observed due to the very closed potential (B/B' and N/N'). The redox signals M/M' and N/N' in Fig. 3(d) indicate the presence of two of the eight expected Zn–Sm intermetallic compounds [40], which could be attributed to the low solubility of Sm in Zn [41]. Thus, the extraction or separation of Sm from molten salts may be accomplished by applying different potentials.

3.2. Square wave voltammetry

SWV generally shows greater sensitivity than CV [42]. As shown in Fig. 4, SWV curves were obtained on the four reactive electrodes in the LiCl–KCl eutectic melt after addition of 1wt% SmCl_3 . Signals corresponding to Sm–M intermetallic compounds, namely, G at -1.67 V, H at -2.15 V, I at -1.78 V, and J(K) at -2.07 V, closely corresponded to the CV results. However, in the red curve of Fig. 4, a new signal O was noted at approximately -1.59 V; this signal could be attributed to the formation of a certain Al–Sm intermetallic compound. Signals obtained during underpotential deposition on the Al electrode were relatively more positive than the potential of Li metal. No Ni–Li or Cu–Li intermetallic compounds were observed; therefore, the signal of Li(I) on the Ni and Cu electrodes is identical to that on the W electrode.

The signals described above were analyzed in detail, and the reactions of Sm on the various reactive electrodes are summarized in Table 2. Due to the underpotential deposition of Sm on the reactive electrodes, the depolarization value (ΔE) is written as [31]:

$$\Delta E = E_R - E_W \quad (1)$$

where E_R and E_W correspond to the reduction potential of Sm(III) on reactive and inert electrodes, respectively. However, E_W could not be determined in the present experiment because Sm(II)/Sm(0) occurs outside of the electro-

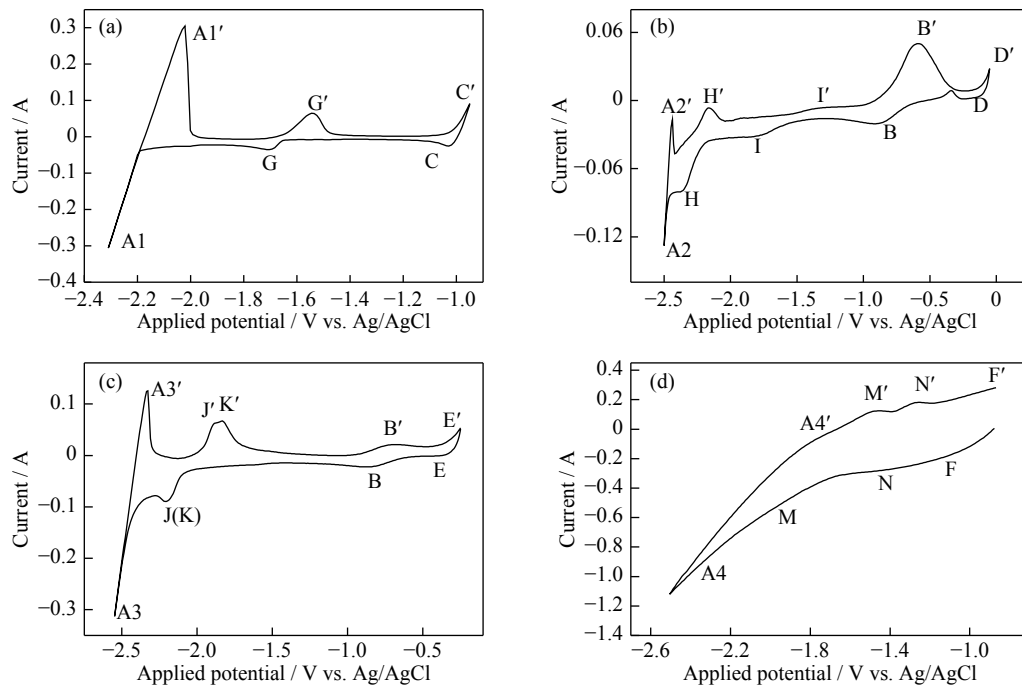


Fig. 3. CV curves obtained on the reactive solid electrodes (a) Al, (b) Ni, and (c) Cu and the liquid electrode (d) Zn in LiCl-KCl-1wt%SmCl₃ melt at 773 K.

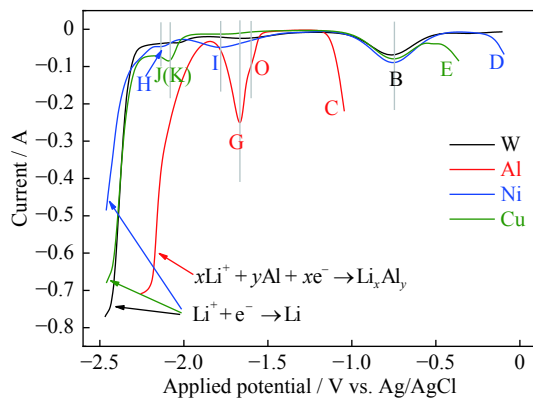


Fig. 4. SWV plots of 1wt% SmCl₃ in LiCl-KCl melt on W, Al, Ni, and Cu electrodes at 773 K and 20 Hz.

chemical window. Therefore, the real depolarization values could not be obtained. The depolarization effects of the reactive electrodes on Sm showed the order Zn > Al > Ni > Cu. Depolarization on reactive electrodes facilitates the deposition of Sm(III) and improves the current efficiency of the system [31]. Reduction potential data can provide a fundamental basis for the extraction of Sm from molten salts on reactive electrodes and preparation of alloy materials.

3.3. Open circuit chronopotentiometry

OCP curves were recorded after each electrolytic process, and the equilibrium potentials of the Sm-M intermetallic compounds were determined [43–44]. First, thin layers of the Sm-M edalloys were fabricated on the reactive electrodes by potentiostatic electrolysis for a certain period of time. Differ-

Table 2. Summary of the CV and SWV results of Sm on various reactive electrodes at 773 K.

Redox couple	Reaction
A0/A0', A2/A2', A3/A3'	$\text{Li}^+ + \text{e}^- \leftrightarrow \text{Li}$
A1/A1'	$x\text{Li}^+ + y\text{Al} + x\text{e}^- \leftrightarrow \text{Li}_x\text{Al}_y$
A4/A4'	$x\text{Li}^+ + y\text{Zn} + x\text{e}^- \leftrightarrow \text{Li}_x\text{Zn}_y$
B/B'	$\text{Sm}^{3+} + \text{e}^- \leftrightarrow \text{Sm}^{2+}$
C/C'	$\text{Al}^{3+} + 3\text{e}^- \leftrightarrow \text{Al}$
G/G', O/O'	$x\text{Sm}^{3+} + y\text{Al} + 3x\text{e}^- \leftrightarrow \text{Sm}_x\text{Al}_y$
D/D'	$\text{Ni}^{2+} + 2\text{e}^- \leftrightarrow \text{Ni}$
H/H', I/I'	$x\text{Sm}^{3+} + y\text{Ni} + 3x\text{e}^- \leftrightarrow \text{Sm}_x\text{Ni}_y$
E/E'	$\text{Cu}^{2+} + 2\text{e}^- \leftrightarrow \text{Cu}$
J/J', K/K'	$x\text{Sm}^{3+} + y\text{Cu} + 3x\text{e}^- \leftrightarrow \text{Sm}_x\text{Cu}_y$
F/F'	$\text{Zn}^{2+} + 2\text{e}^- \leftrightarrow \text{Zn}$
M/M', N/N'	$x\text{Sm}^{3+} + y\text{Zn} + 3x\text{e}^- \leftrightarrow \text{Sm}_x\text{Zn}_y$

ent Sm_xM_y phases were formed following the diffusion of the Sm metal into the M metals by underpotential deposition. The potentiostatic control was then disconnected, and discharging phenomena were recorded as plots of potential versus time. Potential plateaus due to the different states of coexisting phases were also determined [8,45]. The red line in Fig. 5 shows several of these potential plateaus. For example, plateaus 9 at -1.85 V, 11 at -1.6 V, and 14 at -1.40 V correspond to the presence of Al-Sm intermetallic compounds, which is in accordance with the previous literature [26]. The blue line in the same figure shows four plateaus (4 at -2.11 V, 7 at -1.87 V, 10 at -1.74 V, and 15 at -1.36 V) corresponding to Ni-Sm intermetallic compounds. Plateau 7 corresponds to a new Ni-Sm alloy [27]. Sm extraction on the

Cu electrode, which is represented by the green line in Fig. 5, shows four plateaus, namely, 2 at -2.24 V, 5 at -2.03 V, 6 at -1.94 V and 13, at -1.46 V, which are attributed to Cu–Sm intermetallic compounds. Plateaus 6 and 13 indicate new phases compared with those shown in the CV and SWV curves. When Sm metal is deposited on liquid Zn metal, as demonstrated by the pink line in Fig. 5, only plateau 12 is attributed to Zn–Sm intermetallic compound. Plateaus 1, 3, and 8 reflect the equilibrium potentials of Li, Al–Li alloy, and Zn–Li alloy, respectively. The change in potential of Li on the reactive electrodes is in accordance with the SWV findings. The dotted black line 18 corresponds to the reaction Sm(II)/Sm(III), and plateaus 16, 17, 19, and 20 correspond to the open circuit potentials of metallic Zn, Al, Cu, and Ni, respectively.

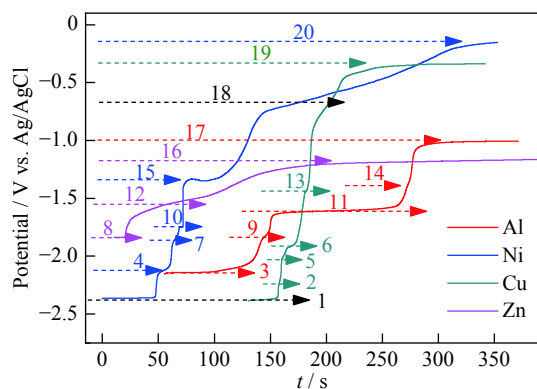


Fig. 5. OCP curves recorded on various reactive electrodes (solid Al, Ni, and Cu and liquid Zn) after potentiostatic electrolysis for a certain period of time in LiCl–KCl–1wt%SmCl₃ melt at 773 K.

Taken together, the results of different electrochemical techniques reveal that the electrochemical signals of all Sm–M intermetallic compounds may be difficult to obtain because of the influence of different thermodynamic and kinetic effects. The phase composition of these compounds was further studied by electrochemical deposition.

3.4. Electroextraction and characterization of the Sm–M alloys

Sm extraction was carried out by galvanostatic and potentiostatic electrolysis on the Al, Ni, Cu, and liquid Zn electrodes to fabricate Sm–M intermetallic compounds.

3.4.1. Electroextraction on the Al electrode

Electroextraction of Sm was carried out on the Al electrode by potentiostatic electrolysis at -1.7 V for 4 h at 773 K. The XRD pattern shown in Fig. 6 reveals the presence of the Al₃Sm phase only. The phase diagram of Al–Sm [46] reveals that the Al-rich intermetallic compound formed above 1351 K is Al₁₁Sm, while that formed below 1408 K is Al₃Sm. Therefore, the signal G in Fig. 3 and Fig. 4 is attributed to Al₃Sm. Compared with the results obtained by CV and SWV,

the potential of signal O is positive than G, in this case, peak O might be related to Al₂Sm. Unmarked peaks in the XRD pattern are attributed to the presence of impurities.

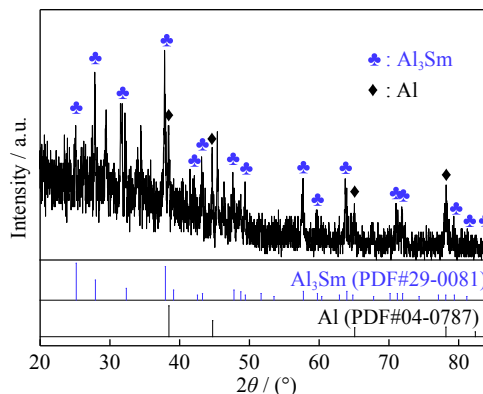


Fig. 6. XRD pattern of the sample prepared by potentiostatic electrolysis at -1.7 V. Working electrode: Al; duration: 4 h; temperature: 773 K.

The product was further analyzed by cross-sectional SEM and EDS, and the results are shown in Fig. 7. The SEM image obtained exhibited distinct light and dark gray zones, which were labeled 001 and 002, respectively. EDS analysis then revealed that these zones correspond to the Al–Sm intermetallic compound and Al matrix, respectively. The ratio of Al to Sm in the deposit is approximately 3/1, which is in accordance with the XRD analysis.

3.4.2. Electroextraction on the Ni electrode

Galvanostatic and potentiostatic electrolysis was conducted to electroextract Sm on the Ni electrode. Different intermetallic compounds were detected. Fig. 8 shows the XRD pattern of the product formed by potentiostatic electrolysis at -1.5 V; the pattern reveals the formation of Ni and Ni₅Sm phases. Therefore, signal I in the CV and SWV curves may indicate the formation of Ni₅Sm. Galvanostatic electrolysis at -0.62 A·cm⁻² was carried out on the Ni electrode for 4 h at 773 K. As can be seen in Fig. 9, another intermetallic compound, namely, Ni₂Sm, was formed. This product is different from the product obtained by potentiostatic electrolysis in Fig. 8.

Fig. 10 shows the SEM–EDS results of the sample in Fig. 8; here, the dark gray (001) and light gray (002) zones correspond to the Ni matrix and alloy phase, respectively. A clear boundary between the Ni matrix and alloy phase could also be observed in the SEM image; this boundary reveals that the alloy phase grows uniformly. Liu *et al.* [28] investigated the coreduction of Ni–Sm alloys in a LiCl–KCl–NiCl₂–SmCl₃ melt by potentiostatic electrolysis and found that Ni₅Sm, Ni₂Sm, and NiSm are the main products of this process.

3.4.3. Electroextraction on the Cu electrode

Sm electroextraction was carried out on the Cu electrode. The Cu–Sm alloy was fabricated by potentiostatic electrolysis at -1.6 V. XRD analysis revealed the presence of Cu₆Sm,

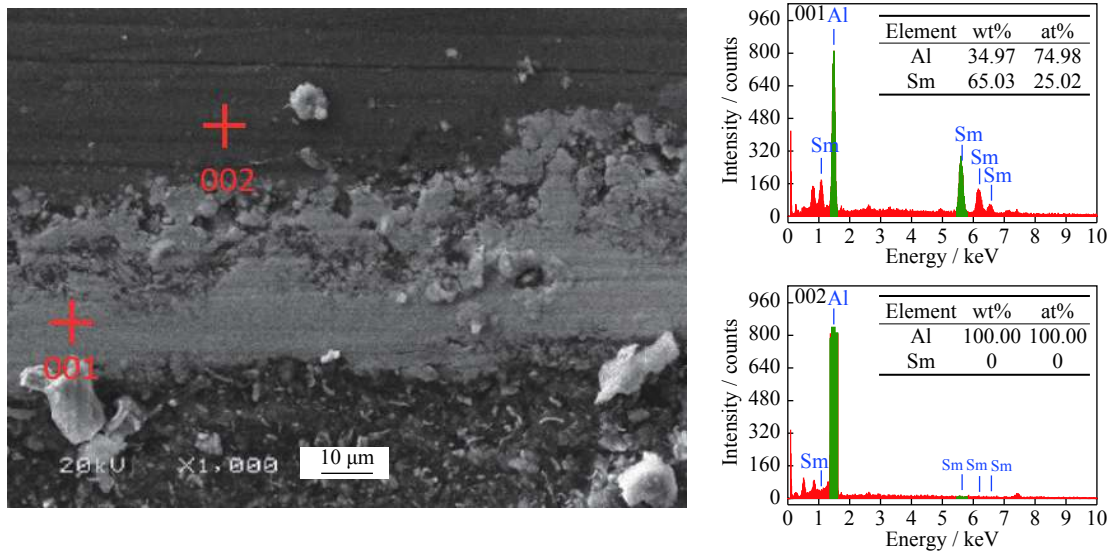


Fig. 7. SEM-EDS analysis results of the sample prepared by potentiostatic electrolysis at -1.7 V. Working electrode: Al; duration: 4 h; temperature: 773 K.

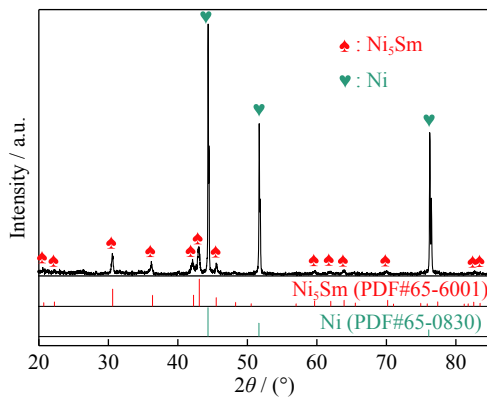


Fig. 8. XRD pattern of the sample prepared by potentiostatic electrolysis at -1.5 V. Working electrode: Ni; duration: 12 h; temperature: 773 K.

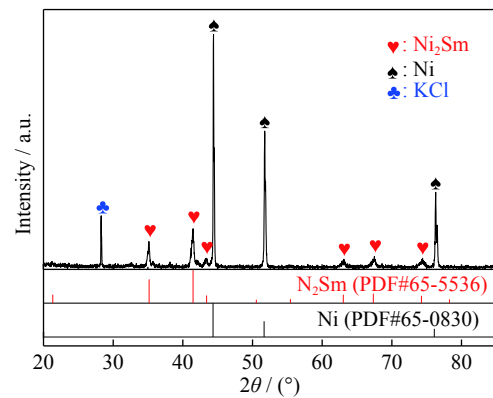


Fig. 9. XRD pattern of the sample prepared by galvanostatic electrolysis at -0.62 A·cm⁻². Working electrode: Ni; duration: 4 h; temperature: 773 K.

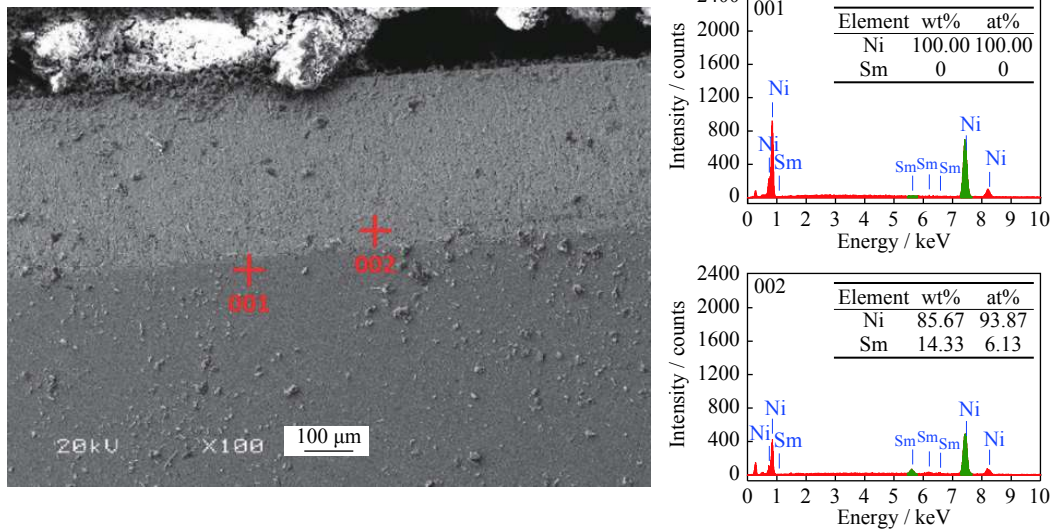


Fig. 10. SEM-EDS analysis results of the sample prepared by potentiostatic electrolysis at -1.5 V. Working electrode: Ni; duration: 12 h; temperature: 773 K.

which is the Cu-rich alloy phase that could be formed from this system (Fig. 11). SEM also revealed a homogeneous alloy phase (Fig. 12).

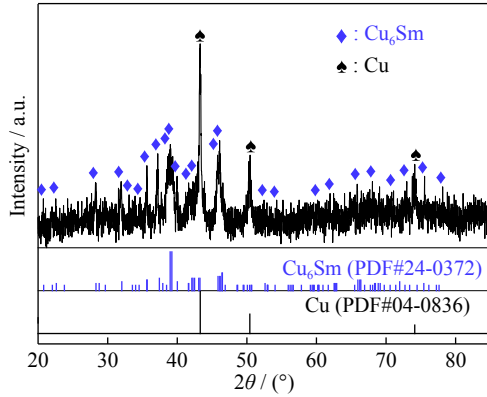


Fig. 11. XRD pattern of the sample prepared by potentiostatic electrolysis at -1.6 V. Working electrode: Cu; duration: 10 h; temperature: 773 K.

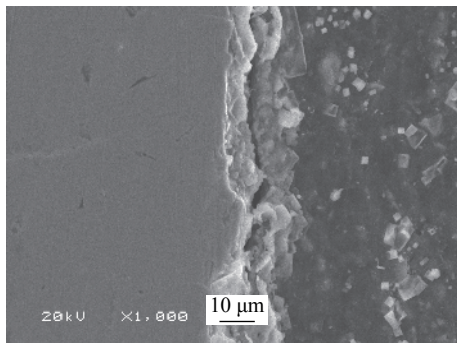


Fig. 12. SEM image of the sample prepared by potentiostatic electrolysis at -1.6 V. Working electrode: Cu; duration: 10 h; temperature: 773 K.

3.4.4. Electroextraction on the liquid Zn electrode

Sm extraction on the liquid Zn electrode was conducted by galvanostatic electrolysis at -0.15 A·cm⁻² and 773 K. A Zn–Sm intermetallic compound could be formed by the saturation of Sm in liquid Zn. Sm₂Zn₁₇ but not SmZn₁₂ was detected by XRD, as shown in Fig. 13. SEM–EDS revealed that the gray zones marked 001 and 002 are related to the Zn–Sm alloy phase, as shown in Fig. 14.

The preparation of Sm–M alloys on different reactive electrodes was achieved by galvanostatic or potentiostatic electrolysis in LiCl–KCl–SmCl₃ melt. During electrolysis, the reactive electrode could be considered the metal-rich material. Thus, M-rich intermetallic compounds may be expected to form prior to other alloy phases. The formation mechanism of these compounds is affected by the thermodynamic, kinetic, and inherent properties of the system components. The M-rich intermetallic compounds Al₃Sm and Cu₆Sm were

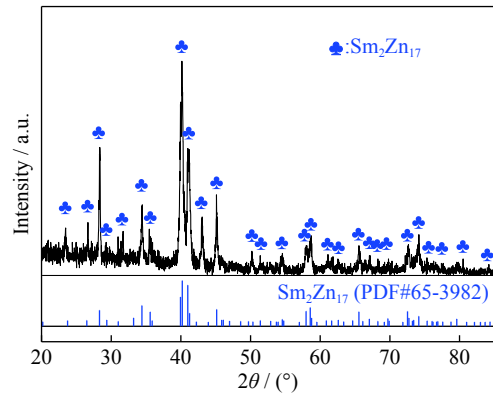


Fig. 13. XRD pattern of the sample prepared by galvanostatic electrolysis at -0.15 A·cm⁻². Working electrode: liquid Zn; duration: 8 h; temperature: 773 K.

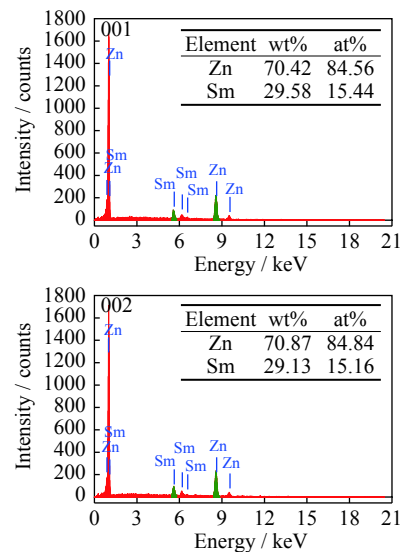
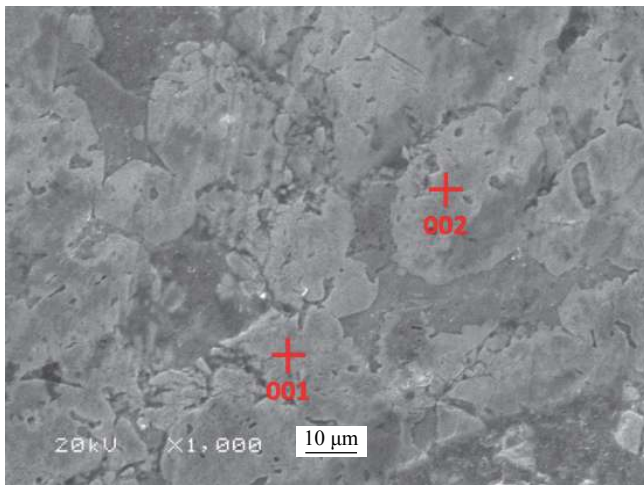


Fig. 14. SEM–EDS analysis results of the sample prepared by galvanostatic electrolysis at -0.15 A·cm⁻². Working electrode: liquid Zn; duration: 8 h; temperature: 773 K.

observed. During extraction of Sm on the Ni electrode, Ni₃Sm and not the expected Ni-richest compound Ni₁₇Sm₂ was obtained, likely because the former is more stable than the latter according to the Ni–Sm phase diagram. Ni₂Sm could also be obtained by galvanostatic electrolysis, during which alloys with the cubic body-centered structure of Fd-3m, such as Ni₂Pr, Ni₂Dy, and Ni₂Yb, are also easily formed [47]. On the Zn electrode, Zn₁₇Sm₂, which is more stable than the Zn-richest compound SmZn₁₁, was obtained. Therefore, while not all possible Sm–M intermetallic compounds are produced, M-rich compounds with the highest stability can be obtained on reactive electrodes.

4. Conclusion

In summary, CV, SWV, and OCP were carried out to investigate the electrochemical behaviors of Sm(III) on four reactive electrodes, including Al, Ni, Cu, and liquid Zn. Extraction of Sm was then conducted by galvanostatic/potentiostatic electrolysis to form Sm–M alloys. The depolarization effect of the reactive electrodes on Sm showed the order Zn > Al > Ni > Cu. Single-phase intermetallic compounds were prepared via potentiostatic or galvanostatic electrolysis on the four reactive electrodes. The XRD patterns of the deposits obtained by underpotential electrolysis revealed that Al₃Sm, Ni₃Sm, and Cu₆Sm could be formed at the applied potentials of –1.7, –1.5, and –1.6 V, respectively. Ni₂Sm and Zn₁₇Sm₂ phases could be fabricated by galvanostatic electrolysis. While not all possible Sm–M intermetallic compounds are formed by this process, M-rich compounds with high stability could be obtained on the reactive electrodes. The results reveal the electrochemical behavior and main products of Sm on reactive electrodes and provide an important reference for the decontamination of Sm in molten salts.

Acknowledgements

This work was financially supported by the National Natural Science Foundation of China (Nos. 21976047, 21790373, and 51774104), the Ph.D. Student Research and Innovation Fund of the Fundamental Research Funds for the Central Universities, China (No. 3072019GIP1011), and the Fundamental Research Funds for the Central Universities, China (No. 3072020CFT1008).

References

- [1] P. Bagri and M.F. Simpson, Activity measurements of gadolinium(III) chloride in molten LiCl–KCl eutectic salt using saturated Gd/GdCl₃ reference electrode, *J. Electrochem. Soc.*, 164(2017), No. 8, p. H5299.
- [2] J.P. Ackerman, Chemical basis for pyrochemical reprocessing of nuclear fuel, *Ind. Eng. Chem. Res.*, 30(1991), No. 1, p. 141.
- [3] J. Zhang, Impurities in primary coolant salt of FHRs: Chemistry, impact, and removal methods, *Energy Technol.*, 7(2019), No. 10, art. No. 1900016.
- [4] Y.L. Liu, L.Y. Yuan, L.R. Zheng, L. Wang, B.L. Yao, Z.F. Chai, and W.Q. Shi, Confirmation and elimination of cyclic electrolysis of uranium ions in molten salts, *Electrochem. Commun.*, 103(2019), p. 55.
- [5] Y. Castrillejo, C. De La Fuente, M. Vega, F. de la Rosa, R. Pardo, and E. Barrado, Cathodic behaviour and oxoacidity reactions of samarium(III) in two molten chlorides with different acidity properties: The eutectic LiCl–KCl and the equimolar CaCl₂–NaCl melt, *Electrochim. Acta*, 97(2013), p. 120.
- [6] G. Cordoba and C. Caravaca, An electrochemical study of samarium ions in the molten eutectic LiCl + KCl, *J. Electroanal. Chem.*, 572(2004), No. 1, p. 145.
- [7] M. Gibilaro, L. Massot, P. Chamelot, and P. Taxil, Co-reduction of aluminium and lanthanide ions in molten fluorides: Application to cerium and samarium extraction from nuclear wastes, *Electrochim. Acta*, 54(2009), No. 22, p. 5300.
- [8] L. Massot, P. Chamelot, and P. Taxil, Cathodic behaviour of samarium(III) in LiF–CaF₂ media on molybdenum and nickel electrodes, *Electrochim. Acta*, 50(2005), No. 28, p. 5510.
- [9] O. Shirai, K. Uozumi, T. Iwai, and Y. Arai, Electrode reaction of the Np³⁺/Np couple at liquid Cd and Bi electrodes in LiCl–KCl eutectic melts, *J. Appl. Electrochem.*, 34(2004), No. 3, p. 323.
- [10] M. Ustundag and R. Varol, Comparison of a commercial powder and a powder produced from Ti–6Al–4V chips and their effects on compacts sintered by the sinter-HIP method, *Int. J. Miner. Metall. Mater.*, 26(2019), No. 7, p. 878.
- [11] G.Y. Lin, X. Tan, D. Feng, J.L. Wang, and Y.X. Lei, Effects of conform continuous extrusion and heat treatment on the microstructure and mechanical properties of Al–13Si–7.5Cu–1Mg alloy, *Int. J. Miner. Metall. Mater.*, 26(2019), No. 8, p. 1013.
- [12] D. Wu, W.L. Wang, L.G. Zhang, Z.Y. Wang, K.C. Zhou, and L.B. Liu, New high-strength Ti–Al–V–Mo alloy: from high-throughput composition design to mechanical properties, *Int. J. Miner. Metall. Mater.*, 26(2019), No. 9, p. 1151.
- [13] Y. Cao, D.D. Zhang, P.J. Zhou, K. Liu, W.Y. Ming, and J. Ma, Reinforcing effect of laminate structure on the fracture toughness of Al₃Ti intermetallic, *Int. J. Miner. Metall. Mater.*, 27(2020), No. 5, p. 678.
- [14] H.B. Sun, W. Wang, Z.J. Yu, Y. Yuan, S. Wang, and S.Q. Jiao, A new aluminium-ion battery with high voltage, high safety and low cost, *Chem. Commun.*, 51(2015), No. 59, p. 11892.
- [15] X.F. Zhang, S.Q. Jiao, J.G. Tu, W.L. Song, X. Xiao, S.J. Li, M.Y. Wang, H.P. Lei, D.H. Tian, H.S. Chen, and D.N. Fang, Rechargeable ultrahigh-capacity tellurium-aluminum batteries, *Energy Environ. Sci.*, 12(2019), No. 6, p. 1918.
- [16] Y. Song, S.Q. Jiao, J.G. Tu, J.X. Wang, Y.J. Liu, H.D. Jiao, X.H. Mao, Z.C. Guo, and D.J. Fray, A long-life rechargeable Al ion battery based on molten salts, *J. Mater. Chem. A*, 5(2017), No. 3, p. 1282.
- [17] H.D. Jiao, C. Wang, J.G. Tu, D.H. Tian, and S.Q. Jiao, A rechargeable Al-ion battery: Al/molten AlCl₃–urea/graphite, *Chem. Commun.*, 53(2017), No. 15, p. 2331.
- [18] Y. Gao, Y.K. Shi, X.L. Liu, C. Huang, and B. Li, Cathodic behavior of samarium(III) and Sm–Al alloys preparation in fluorides melts, *Electrochim. Acta*, 190(2016), p. 208.
- [19] M.L. Zhang, Y.D. Yan, W. Han, X. Li, Z.Y. Hou, Y. Tian, K. Ye, L.H. Bao, X.D. Li, and Z.J. Zhang, A new approach for the preparation of variable valence rare earth alloys from nano rare earth oxides at a low temperature in molten salt, *RSC Adv.*, 2(2012), No. 4, p. 1585.

- [20] K. Liu, Y.L. Liu, L.Y. Yuan, H. He, Z.Y. Yang, X.L. Zhao, Z.F. Chai, and W.Q. Shi, Electroextraction of samarium from Sm_2O_3 in chloride melts, *Electrochim. Acta*, 129(2014), p. 401.
- [21] Y. Castrillejo, P. Fernández, J. Medina, P. Hernández, and E. Barrado, Electrochemical extraction of samarium from molten chlorides in pyrochemical processes, *Electrochim. Acta*, 56(2011), No. 24, p. 8638.
- [22] P. Chamelot, L. Massot, C. Hamel, C. Nourry, and P. Taxil, Feasibility of the electrochemical way in molten fluorides for separating thorium and lanthanides and extracting lanthanides from the solvent, *J. Nucl. Mater.*, 360(2007), No. 1, p. 64.
- [23] Y.H. Liu, S. Zhang, W.H. Zhong, G.K. Cui, Y.C. Wang, Y. Dai, X.H. Cao, Y.Q. Wang, Z.B. Zhang, and Y.H. Liu, Electrochemical extraction of Sm(III) on active Ni electrode fabricated Sm–Ni alloys, *J. Radioanal. Nucl. Chem.*, 322(2019), No. 2, p. 1003.
- [24] P. Taxil, L. Massot, C. Nourry, M. Gibilaro, P. Chamelot, and L. Cassayre, Lanthanides extraction processes in molten fluoride media: Application to nuclear spent fuel reprocessing, *J. Fluorine Chem.*, 130(2009), No. 1, p. 94.
- [25] Y.L. Liu, L.Y. Yuan, K. Liu, G.A. Ye, M.L. Zhang, H. He, H.B. Tang, R.S. Lin, Z.F. Chai, and W.Q. Shi, Electrochemical extraction of samarium from LiCl–KCl melt by forming Sm–Zn alloys, *Electrochim. Acta*, 120(2014), p. 369.
- [26] D.B. Ji, Y.D. Yan, M.L. Zhang, X. Li, X.Y. Jing, W. Han, Y. Xue, Z.J. Zhang, and T. Hartmann, Electrochemical preparation of Al–Sm intermetallic compound whisker in LiCl–KCl Eutectic Melts, *Electrochim. Acta*, 165(2015), p. 211.
- [27] T. Iida, T. Nohira, and Y. Ito, Electrochemical formation of Sm–Ni alloy films in a molten LiCl–KCl– SmCl_3 system, *Electrochim. Acta*, 46(2001), No. 16, p. 2537.
- [28] Y.H. Liu, Y.D. Yan, M.L. Zhang, J.N. Zheng, P. Wang, T.Q. Yin, Y. Xue, X.Y. Jing, and W. Han, Electrochemical synthesis of Sm–Ni alloy magnetic materials by Co-reduction of Sm(III) and Ni(II) in LiCl–KCl– SmCl_3 – NiCl_2 melt, *J. Electrochem. Soc.*, 163(2016), No. 13, p. D672.
- [29] Y.H. Liu, Y.D. Yan, M.L. Zhang, D.B. Ji, P. Li, T.Q. Yin, P. Wang, Y. Xue, X.Y. Jing, W. Han, M. Qiu, and D.H. H, Electrochemical synthesis of Sm–Cu dendritic metal catalysts by Co-reduction of Sm(III) and Cu(II) in LiCl–KCl– SmCl_3 – CuCl_2 melt, *J. Alloys Compd.*, 772(2019), p. 978.
- [30] H.J. Zhao, H.W. Xie, X.B. Zhou, J.K. Qu, Z.Q. Zhao, Q.S. Song, Z.Q. Ning, P.F. Xing, and H.Y. Yin, Engineering the electrochemical reduction of carbon and silica in molten CaCl_2 : Manipulation of the electrolytic products, *J. Electrochem. Soc.*, 166(2019), No. 4, p. E137.
- [31] S.L. Du, M.S. Zhou, and D.X. Tang, Depolarization of rare-earth metals on a liquid aluminum cathode in molten chlorides, *Chin. J. Appl. Chem.*, 4(1987), No. 2, p. 65.
- [32] K. Liu, Y.L. Liu, Z.F. Chai, and W.Q. Shi, Evaluation of the electroextractions of Ce and Nd from LiCl–KCl molten salt using liquid Ga electrode, *J. Electrochem. Soc.*, 164(2017), No. 4, p. D169.
- [33] Y.L. Liu, G.A. Ye, K. Liu, L.Y. Yuan, Z.F. Chai, and W. Shi, Electrochemical behavior of La (III) on the zinc-coated W electrode in LiCl–KCl eutectic, *Electrochim. Acta*, 168(2015), p. 206.
- [34] D. Pletcher, R. Greff, R. Peat, L. Peter, and J. Robinson, *Instrumental Methods in Electrochemistry*, Woodhead Publishing Limited, Pennsylvania, 2001.
- [35] I. Barin and G. Platzki, *Thermochemical Data of Pure Substances*. 3rd ed, VCH Verlagsgesellschaft mbH, Weinheim, 1995.
- [36] T.V. Kulikova, A.V. Maiorova, V.A. Bykov, and K.Y. Shun-yaev, Thermodynamic properties of melts based on the Al–Sm system, *Russ. J. Phys. Chem. A*, 86(2012), No. 8, p. 1185.
- [37] X.P. Su, W.J. Zhang, and Z.M. Du, A thermodynamic assessment of the Ni–Sm system, *J. Alloys Compd.*, 278(1998), No. 1–2, p. 182.
- [38] W. Zhuang, Z.Y. Qiao, S. Wei, and J. Shen, Thermodynamic Evaluation of the Cu–R (R: Ce, Pr, Nd, Sm) Binary Systems, *J. Phase Equilib.*, 17(1996), No. 6, p. 508.
- [39] H. Konishi, T. Nohira, and Y. Ito, Formation and phase control of Dy alloy films by electrochemical implantation and displacement, *J. Electrochem. Soc.*, 148(2001), No. 7, p. C506.
- [40] B.R. Jia, L.G. Zhang, G.X. Huang, H.Y. Qi, H. Yang, L.B. Liu, Z.P. Jin, and F. Zheng, Thermodynamic assessment of the Sm–Zn binary system, *J. Alloys Compd.*, 473(2009), No. 1–2, p. 176.
- [41] P. Chiotti and J.T. Mason, Phase relations and thermodynamic properties for the samarium-zinc system, *Trans. Met. Soc. AIME*, 239(1967), No. 4, p. 547.
- [42] S.L. Li, Y.S. Che, J.X. Song, C.Y. Li, Y.C. Shu, J.L. He, and B. Yang, Electrochemical studies on the redox behavior of Zr(IV) in the LiCl–KCl eutectic molten salt and separation of Zr and Hf, *J. Electrochem. Soc.*, 167(2020), No. 2, art. No. 023502.
- [43] Y. Castrillejo, P. Hernández, R. Fernández, and E. Barrado, Electrochemical behaviour of terbium in the eutectic LiCl–KCl in Cd liquid electrodes.- Evaluation of the thermochemical properties of the TbCd_x intermetallic compounds, *Electrochim. Acta*, 147(2014), p. 743.
- [44] T.Q. Yin, Y. Xue, Y.D. Yan, Y.H. Zheng, Y.L. Song, G.L. Wang, M.L. Zhang, M. Qiu, and D.H. Hu, Electrochemical synthesis and thermodynamic properties of Pr–Ni intermetallic compounds in a LiCl–KCl– NiCl_2 – PrCl_3 Melt, *ChemElectroChem*, 6(2019), No. 3, p. 876.
- [45] Y. Castrillejo, M. Bermejo, P.D. Arocas, A. Martínez, and E. Barrado, Electrochemical behaviour of praseodymium(III) in molten chlorides, *J. Electroanal. Chem.*, 575(2005), No. 1, p. 61.
- [46] L.L. Jin, Y.B. Kang, P. Chartrand, and C.D. Furst, Thermodynamic evaluation and optimization of Al–La, Al–Ce, Al–Pr, Al–Nd and Al–Sm systems using the modified quasichemical model for liquids, *Calphad*, 35(2011), No. 1, p. 30.
- [47] T.Q. Yin, Y. Liang, J.M. Qu, P. Li, R.F. An, Y. Xue, M.L. Zhang, W. Han, G.L. Wang, and Y.D. Yan, Thermodynamic and electrochemical properties of praseodymium and the formation of Ni–Pr intermetallics in LiCl–KCl melts, *J. Electrochem. Soc.*, 164(2017), No. 13, p. D835.